Indian Journal of Fundamental and Applied Life Sciences ISSN: 2231– 6345 (Online)
An Open Access, Online International Journal Available at www.cibtech.org/sp.ed/jls/2014/04/jls.htm
2014 Vol. 4 (S4), pp. 1448-141462/Palandi et al.
Research Article

NUMERICAL SIMULATION OF FLOW AND HEAT TRANSFER OF TURBULENT NANOFLUID FLOW IN A TRIANGULAR ROD BUNDLE

Saed Jalili Palandi, *Mazaher Rahimi-Esbo and Reza Mohammadyari
Young Researchers and Elite Club, Buin zahra Branch, Islamic Azad University, Buin zahra, Iran
**Author for Correspondence*

ABSTRACT
In this study the flow field of VVER-440 fuel rod bundle is numerically investigated, focusing on its heat transfer characteristics. The fuel rod bundle contains 60 fuel rods with length of 960 mm and 4 spacer grids. In VVER-440 fuel rod bundle the coolant fluid (water) is in high pressure and temperature condition. In order to improve its thermal properties, water-AL2O3 nanofluid is used. In this literature, the effects of diameter and volume fraction of nanoparticles on thermo-hydraulic parameters are studied. To perform correct calculation, different turbulence models and grid qualities of fuel rod bundle are studied and results are compared with reference results. The Brownian motions of nanoparticles have been considered to determine the thermal conductivity and dynamic viscosity of Al2O3-Water nanofluid, which depend on the temperature. The results show that (i) a significant enhancement of heat transfer coefficient in studied fuel rod bundle due to suspension of Al2O3 nanoparticles in the base fluid in comparison with pure water is obtained, (ii) enhancement of heat transfer is intensified with increasing the volume fraction of nanoparticles, (iii) increasing the volume fraction of nanoparticles leads to higher pressure drop, (iv) with decreasing particle diameters the heat transfer coefficient increases for Al2O3-water nanofluid.

Keywords: *Nanofluid, Heat Transfer Coefficient, Rod Bundle, Volume Fraction, Particle Diameter*

Nomenclature

$C_{\varepsilon 1}, C_{\varepsilon 2}, C_{\mu}$	constants in the model transport equations	t	time , (s)
C_p	specific heat (kJ/kg.K)	V_b	Brownian velocity of nanoparticles, (m/s)
d_f	diameter of base fluid molecules (m)	**Greek symbols**	
d_p	average diameter of nanoparticles (m)	α	thermal diffusivity (m^2/s)
F_1	blending functions in k-ω SST model	δ	center-to-center distance of nanoparticles (m)
h	height of rod bundle (mm)	ε	turbulent dissipation rate (m^2/s^3)
h_{ave}	heat transfer coefficient ($W/m^2.k$)	μ	dynamic viscosity, (*kg/m.s*)
K_b	Boltzmann number ($=1.3807\times10^{-23}$ J/K)	ρ	density,(kg/m^3)
k	turbulence kinetic energy, (m^2/s^2)	ω	specific dissipation rate of turbulent kinetic energy (1/s)
L_f	free average distance of water molecules (m)	**Subscripts**	
N	parameter for adapting the results with experimental data	ave	average
pr	Prandtl number of nanofluid	f	Base fluid

q''	uniform heat flux (W/m^2)	nf	nanofluid
Re	Reynolds number	P	Particle
T	temperature, (K)	w	wall

INTRODUCTION

In nuclear reactors, obtaining a detailed understanding of the flow field, coolant fluid temperature and pressure is very important. In pressurized water reactor, control of coolant fluid temperature and pressure is very important for the viewpoint of safety. For example, a spot with high temperature in fuel rods cladding can be very dangerous. Pressurized water reactors (PWR) are the most common nuclear reactors that use water as coolant fluid. In these reactors because of high water pressure, the boiling temperature is very high and the fluid is always liquid, thus the reactors coolant fluid is known as a high pressure and temperature water.VVER-440 reactor is one type of pressurized water reactors that has a hexagonal fuel assembly. Recently, many experimental and numerical studies on the flow field and heat transfer in fuel rods bundle have been done.

Conner *et al.,* (2010) presented a CFD methodology to model single-phase, steady-state conditions in PWR fuel assemblies and performed experiments to validate the CFD methodology for this fuel assemblies. Their numerical simulation results were compared to experimental results and concluded that the proposed CFD model is suitable to predict the fluid behavior in PWR fuel rod bundle. Tóth *et al.,* (2006) numerically simulated a 60 degree sector of VVER-440 fuel rod bundle includes 21 fuel rods and 4 spacer grids. Three turbulence models for the flow in fuel rod bundle channels were considered and temperature of fuel rods cladding, cooling fluid temperature, coolant fluid pressure, turbulent kinetic energy and heat transfer coefficient were investigated. The results indicated that by using k-Omega model, higher heat transfer coefficient was obtained than other turbulence models. Aszódi *et al.,* (2008) investigated the flow and heat transfer process in a single sub channel (triangular lattice) and in rod bundle sections of VVER-440 reactors. Their mesh sensitivity study showed that the suitable mesh resolution is very important to correctly predict the turbulence quantities in a subchannel. The study indicated that the results calculated using the BSL Reynolds stress model were in best agreement with experimental data.

In some studies, the mixing vanes role for enhancing the heat transfer coefficient has been investigated. Abdi *et al.,* (2012) investigated the role of long and short mixing vanes in VVER-440 fuel rod bundle with length of 240 and 960 mm to increase the heat transfer coefficient. Their results indicated that short length mixing vanes produce higher heat transfer coefficient than long length mixing vanes. Byung (2009) numerically and experimentally studied flow field and heat transfer in 2×3 rod bundles with different mixing vanes. Three mixing vanes were simulated and the effects of critical heat flux were investigated to obtain optimum mixing vane in different operating conditions. The results showed that near the PWR operating conditions, the hybrid vane showed the best CHF enhancement. Cui *et al.,* (2003) evaluated the effects of mixing vane shape on the flow structure and heat transfer downstream of mixing vane in a subchannel of fuel assembly, by obtaining velocity and pressure fields, turbulent intensity, flow mixing factors, heat transfer coefficient, and friction factor using three-dimensional RANS analysis .In their study numerical results with three turbulence models were compared with experimental data. They concluded that standard k–ε model showed the best performance in the aspects of accuracy and computational time. In many studies on VVER-440 fuel rod bundle, it was attempted to increase the heat transfer coefficient by factors such as optimization array of fuel rods and putting mixing vans on the spacer grids. Both techniques are related to the geometry of rods bundle. Another way to increase the heat transfer in rod bundle is improving the thermal properties of coolant fluid.

Consequently, different techniques have been suggested to increase the heat transfer properties of fluids. Researchers have also attempted to enhance the thermal conductivity of base fluids by suspending micro- or larger-sized solid particles in fluids, since the thermal conductivity of solid is typically higher than that of liquids. However, due to the large size and high density of the particles, there is no proper technique to

avoid the solid particles from settling out of suspension. Therefore, fluids with dispersed coarse-grained particles have not yet been commercialized.

Fluids with suspended nanoparticles are called nanofluid, a term proposed by Choi (1995) of the Argonne National Laboratory, USA. This new type of fluid is manufactured by dispersing a small amount of solid nanoparticles in conventional heat transfer fluids. Some advantages of nanofluids that make them useful are: high effective thermal conductivity, high stability, less clogging and abrasion. The much larger relative surface area of nanoparticles, compared to those of conventional particles, should not only significantly improve the heat transfer capabilities, but also should increase the stability of the suspensions. Also, nanofluids due to containing tiny particles can improve abrasion-related properties as compared to the conventional solid/fluid mixtures. To explain the reasons for the anomalous increase of the thermal conductivity in nanofluid, Keblinski *et al.,* (2002) and Eastman *et al.,* (2004) proposed four possible mechanisms: Brownian motion of the nanoparticles, molecular-level layering of the liquid at the liquid/particle interface, the nature of heat transport in the nanoparticles, and the effects of nanoparticles clustering. Ghaffari *et al.,* (2010) numerically studied turbulent mixed convection heat transfer of the AL_2O_3-water nanofluid in a horizontal curved tube using two phase model approach. The results indicated that at the low Grashof number, the turbulent intensity increased with increasing nanoparticle volume fraction but at the higher Grashof number using higher nanoparticle concentration, decreased the flow turbulent intensity across the vertical plane.

Behzadmehr *et al.,* (2007) simulated turbulent forced convection of a nanofluid in a circular tube. Two phase mixture models were applied for calculations. The results indicated that adding 1% nanoparticles increased the Nusselt number by more than 15%. The study showed that in order to improve accuracy of calculations, effective physical properties must be considered for nanofluid instead of volume weighted average of particles and fluid properties.

Cooling applications of nanofluid showed that nanofluid can be applied to power plant cooling and safety systems due to their enhanced properties such as thermal conductivity. Several investigations related to practical application of nanofluid in nuclear reactor technology have been performed. Buongiorno *et al.,* (2005) investigated feasibility of using nanofluids in light water reactors. The analysis indicated that the use of nanofluid can increase the in-vessel retention capability of nuclear reactors as much as 40%. Hadad *et al.,* (2010) investigated the effects of using nanofluid in VVER-1000 reactor on neutronic parameters changes. They reported that AL_2O_3-water nanofluid has the lowest rate of multiplication factor droplet in comparison to copper oxide and zirconia nanoparticles. Zarifi *et al.,* (2013) performed a thermal–hydraulic analysis of nanofluid as the coolant fluid in VVER-1000 reactor core using the porous media approach. They studied water-based nanofluids containing various volume fractions of AL_2O_3 and TiO_2 nanoparticles. The results showed that the temperature of the coolant fluid has been increased with the concentration of nanoparticles.

In this study, water-AL_2O_3 nanofluid is considered as the cooling fluid and the effects of nanoparticles diameter and volume fraction on the heat transfer coefficient and pressure drop of fluid flow in VVER-440 rod bundle channels is studied.

Model Description

Fuel assemblies of the VVER-440 type reactors consist of three main parts: assembly legs, rod bundles and assembly heads. The simulated rod bundles include 61 fuel rods arranged in a triangular configuration, 4 spacer grids and a central tube for the self-powered neutron detectors. The height of fuel rod bundle is 960 mm. The pitch of fuel rods and spacer grids are 12.2 and 240 mm, respectively, and also the outer diameter of the fuel rods is 9.1 mm. Figure 1 shows this rod bundle and for better visibility, the rod bundle is shown semi-transparent.

In each spacer grid, each rod is kept by three holder springs with hexagonal geometry. The constant distance between the fuel rods is maintained by spacer grids placed along the length of the rod bundle. The coolant media flows axially in the sub-channels formed between the rods. Figure 2 represents the spacer grids of the full model. The height of spacer grids, thickness of holder spring and thickness of other parts of spacer grids are 10, 0.25 and 0.5 mm, respectively.

Since the fuel rod bundle is hexagonal and the boundary conditions are symmetric, the size and time of numerical computation can be decreased by modeling a 60 degree segment of fuel rod bundle and the results would be closer to reality.

Figure 3 illustrates the 60 degree segment of fuel rod bundle. This geometry includes 12 fuel rods (8 full rods and 4 half rods), central tube, 4 spacer grids and walls of the shroud. Wall thickness of the shroud was ignored and the wall was modeled as a thin surface. This simplification is logical, since considering the thickness of the shroud about 2 mm, the thermal conductivity of the shroud material is relatively high.

The spacer grids enhance the turbulence of the flow, therefore the heat transfer coefficient increases. Also, using the spacer grids increases the pressure drop due to blocking higher area of flow sub-channels.

Figure 4 illustrates the 60 degree segment of spacer grid. In Figure 4 exact position of fuel rods and sub-channels in spacer grids are shown by putting a fuel rods.

Simulation and Boundary Conditions

Numerical investigation requires sufficient definition of the boundary conditions. In this effort, the coolant media is introduced to the domain with the velocity of 3.25 m/s and temperature of 540°K. The physic of the problem denotes the turbulence condition in which turbulence intensity is considered close to 3.5%. The hydraulic diameter of the bundle is 7.782 mm.

The coolant media is assumed to be water in about 124bar pressure. No slip adiabatic condition is considered for the walls of the shroud, whereas for the walls of the rod, no slip boundary condition with constant heat flux about 1047340 W/m^2 is set. At the outlet of the rod bundle, the pressure was defined to be zero. With respect to the average value of the axial heat flux in modeling of the domain in the VVER-440 reactor at full power (1375 MW), the maximal core heat flux doesn't change sensibly from the average amount.

Heat conduction in the spacer grids was ignored since the walls were very thin (0.25–0.5mm) and the contact areas between them and fuel rods are rather small. All walls are considered to be smooth, and no roughness was determined for them. Symmetry boundary conditions are defined on symmetry planes. The solid parts are assumed to be Zirconium metal. Figure 5 shows some boundary conditions schematically for a section of this fuel rod bundle.

In order to define a suitable mesh resolution for the rod bundle geometry, mesh sensitivity study should be performed. Hence, three mesh numbers were generated applying different mesh densities on the spacer grid parts while maintaining the remaining global mesh spacing unchanged.

Figures 6, 7 and 8 illustrate cladding average temperature, heat transfer coefficient and average static pressure of coolant media at different mesh resolutions, respectively. Results indicated that there was little grid influence for grid numbers greater than 2,199,607 elements; therefore this grid number is used for this investigation.

In Figure 6 it can be seen that the cladding average wall temperature decreases at the spacer grid. When the coolant flows into the holes of the spacer grid the velocity and the turbulence kinetic energy grow rapidly, therefore the heat transfer conditions improve (see heat transfer coefficient in Figure 7) and the temperature of the cladding decreases suddenly. Behind the spacer grids, the temperature of the cladding rises again, because the average turbulence kinetic energy decays. Therefore, the conditions of the heat transfer become worse and the heat transfer coefficient decreases.

Figure 8 shows four local pressure drops. The explanation of this behavior is that the coolant flow velocity increases in the spacer grids due to contraction and this causes a local pressure drop.

Behind the spacer grids, the flow velocity reduces rapidly and the static pressure increases to a value which is less than the amount it was in front of the spacer grids, because that spacer grids cause a separation loss.

Figures 6, 7 and 8 confirmed that the grid number of about 2,199,607 elements satisfies the calculations for this study.

Turbulence Models Study

In this paper turbulence is modeled with the $k-\omega$ SST model. In the $k-\omega$ SST model transport equations for the turbulence kinetic energy and turbulence dissipation are as following:

$$\frac{\partial(\rho k)}{\partial t}+\frac{\partial(\rho U_j k)}{\partial X_j}=\frac{\partial}{\partial X_j}\left[\left(\mu+\frac{\mu_t}{\sigma_k}\right)\frac{\partial k}{\partial X_j}\right]+P_k-\rho\varepsilon \tag{1}$$

$$\frac{\partial(\rho\varepsilon)}{\partial t}+\frac{\partial(\rho U_j\varepsilon)}{\partial X_j}=\frac{\partial}{\partial X_j}\left[\left(\mu+\frac{\mu_t}{\sigma_\varepsilon}\right)\frac{\partial\varepsilon}{\partial X_j}\right]+\frac{\varepsilon}{k}\left[C_{\varepsilon 1}P_k-C_{\varepsilon 2}\rho\varepsilon\right] \tag{2}$$

The turbulent viscosity, μ_t , is computed by combining turbulence kinetic energy and turbulence dissipation as follows:

$$\mu_t=\rho C_\mu\frac{k^2}{\varepsilon} \tag{3}$$

In the $k-\omega$ SST model, transport equations for the turbulence kinetic energy and turbulence dissipation are as following:

$$\frac{\partial(\rho k)}{\partial t}+\frac{\partial(\rho U_j k)}{\partial X_j}=\frac{\partial}{\partial X_j}\left[\left(\mu+\frac{\mu_t}{\sigma_k}\right)\frac{\partial k}{\partial X_j}\right]+P_k-\beta'\rho k \tag{4}$$

$$\frac{\partial}{\partial t}(\rho\omega)+\frac{\partial\left(\rho U_j\omega\right)}{\partial X_j}=\frac{\partial}{\partial x_j}\left[(\mu+\frac{\mu_t}{\sigma_\omega})\frac{\partial\omega}{\partial x_j}\right]+\alpha\frac{\omega}{k}P_k-\beta\rho\omega+(1-F_1)\frac{2\rho}{\sigma_{\omega 2}}\frac{\partial k}{\partial X_j}\frac{\partial\omega}{\partial X_j} \tag{5}$$

Blending function of F1 is used in the model which activates the $k-\omega$ model close to the wall and $k-\varepsilon$ model in the outer region.

All equations are solved using control volume formulation through the use of an open-source CFD package Open FOAM (2011). The pressure field and velocity field are coupled together through the SIMPLE algorithm. Also, second order upwind method is used for the convective and diffusive terms.

Average pressure and average turbulence kinetic energy of coolant fluid calculated from $k-\varepsilon$ Standard and $k-\omega$ SST models are illustrated in Figures 9 and 10, respectively.

Figure 9 shows four local pressure drop. The explanation of this behavior is that the coolant flow velocity increases in the spacer grids due to contraction and it causes a local pressure drop. Behind the spacer grids the flow velocity reduces rapidly and the static pressure increases to a value which is less than it was in front of the spacer grids, because that spacer grids cause a separation loss.

Figure 10 shows four local growth of average turbulent kinetic energy. This is due to the barrier (spacer grid) in flow direction, which increases the flow turbulence feature, and therefore the turbulent kinetic energy intensifies suddenly.

Figures 9 and10 indicated that result obtained from $k-\varepsilon$ Standard and $k-\omega$ SST models are close together and negligible differences are due to modeling and calculating errors. In the next steps calculations are carried out using the k-ω SST turbulence model.

Figure 11 indicates the contours of average turbulence kinetic energy of flow in sub-channels flow before the first spacer grid (h=110 mm), (h=120 mm) and after (h=130 mm). It is obvious that turbulence kinetic energy is increased at the spacer grid.

Coolant fluid with specific temperature enters to rod bundle channels and in the flow direction its temperature increases with enhancing the height. Coolant fluid reaches to highest temperature at outlet (the highest height). The outlet temperature distribution of the coolant fluid is presented in Figure 12. It can be seen that the coolant temperature increases with enhancing the height.

Average heat transfer coefficient is an important parameter in examining rod bundle performance that is calculated as following:

$$h_{ave}=\frac{\dot{q}_W''}{T_W-T_{ave}} \tag{6}$$

T_w ,T_{ave} and $\dot{q}_W''$ are the rod cladding temperature, average of coolant fluid temperature and heat flux of the fuel rods (1,047,340 W/m^2), respectively.

Average heat transfer coefficient of fuel rod bundle is presented in Figure 13. It can be seen that the heat transfer coefficient enhanced at the spacer grids. Figure 14 indicated that the cladding temperature decreased at the spacer grids. This is because when coolant fluid flows into the holes of the spacer grid, the turbulence intensity rises rapidly (see Figure 10) therefore the heat transfer coefficient improves (see figure 13) and according to equation (6) the cladding temperature decreases (see figure 14).

Figures 9, 10, 13 and 14 indicated that result obtained from $k-\varepsilon$ Standard and $k-\omega$ SST models are close together. In the next steps calculations are carried out using the k-ω SST turbulence model.

Validation

In order to analyze the precision of the model assumptions and the numerical procedure, obtained results are compared to results of Abdi *et al.*, (2012). In this step, the fluid inlet velocity is considered to be 3.25 m/s. As shown in Figures 15 and 16, the results are in good agreement with numerical results of Abdi *et al.*, (2012).

The Role of Nanofluids in Heat Transfer

To study the role of nanofluids in heat transfer, many parameters should be considered. Nanofluids thermal properties are related to the temperature, mean nanoparticle diameter, nanoparticle volume fraction, nanoparticle density and the based fluid physical properties.

Janga *et al.*, (2004) showed that as the temperature increases, the effect of nanoparticles on enhancing thermal conductivity intensifies. So it can be said that as the VVER-440 fuel rod bundle works in high temperature condition, using the nanofluids in this rod bundle can be very effective.

In this study water-AL_2O_3 nanofluid is considered as coolant fluid. The nanofluid is assumed as a single phase and incompressible fluid. For the numerical calculations, thermal conductivity, viscosity, density and heat capacity of the nanofluid is embedded to the open source code.

The thermal conductivity of the nanofluid is calculated from Chon *et al.*, (2005), which is expressed in the following form:

$$\frac{K_{nf}}{K_f} = 1 + 46.7\phi^{0.746}\left(\frac{d_f}{d_P}\right)^{0.369} \times \left(\frac{K_P}{K_f}\right)^{0.7476} \mathrm{Pr}_f^{\,0.9955}\,\mathrm{Re}_P^{\,1.2321} \tag{7}$$

$$\mathrm{Pr}_f = \frac{\mu_f}{\rho_f \alpha_f} \tag{8}$$

$$\mathrm{Re}_P = \frac{\rho_f K_b T}{3\pi\mu^2 L_f^{\,2}} \tag{9}$$

Where K_b is the Boltzmann constant, 1.3807×10^{-23} and L_f is the free average distance of water molecules that according to suggestion of Chon *et al.*, (2005) is taken as 0.17 nm . Minister *et al.*, (2009) also approved the accuracy of this model.

The viscosity of the nanofluid is approximated as viscosity of the base fluid μ_f containing dilute suspension of fine spherical particles, as given by Masoumi *et al.*, (2009).

$$\frac{\mu_{nf}}{\mu_f} = 1 + \frac{\rho_P V_d d_P^{\,2}}{72N\delta} \tag{10}$$

$$V_b = \left(\frac{1}{d_P}\right)\sqrt{\frac{18K_b T}{\pi\rho_P d_P}} \tag{11}$$

$$N = (C_1 d_p + C_2)\phi + (C_3 d_p + C_4) \tag{12}$$

$$\delta = \sqrt[3]{\frac{\pi}{6\phi}} \times d_p \tag{13}$$

N is a parameter for adapting the results with experimental data, where

$C_1 = -1.133\times10^{-6}$, $C_2 = -2.771\times10^{-6}$, $C_3 = 9\times10^{-8}$, $C_4 = -3.93\times10^{-7}$

The density and specific heat capacity of the nanofluid are calculated by using the Pak and Cho (1998) correlations, which are defined as follows:

$$\rho_{nf} = \phi\rho_P + (1-\phi)\rho_f \tag{14}$$

$$Cp_{nf} = \frac{(1-\phi)\rho_f Cp_f + \phi\rho_P Cp_P}{\rho_{nf}} \tag{15}$$

Table (1) shows the thermo-physical properties of AL_2O_3 at temperature of 540°k and water at pressure of 12.4 MPa and temperature of 540°k.

In this study water-AL_2O_3 nanofluid is considered as coolant fluid and effects of volume fraction and diameter of nanoparticles on the heat transfer coefficient and pressure drop are investigated. Average heat transfer coefficient is one of the important parameters in VVER-440 rod bundle that can be calculated from Equation (6).

Figure 17 shows the changes of heat transfer coefficient at different volume fractions and different Reynolds numbers at nanoparticles diameter of 50nm. In table (2) total mean of heat transfer coefficient in rod bundle, at different Reynolds numbers is presented. As it can be seen, the heat transfer coefficient increases with enhancement of the nanoparticle volume fraction for all Reynolds numbers. Results show that the addition of solid nanoparticles to the base fluid has led to an increase in mean heat transfer coefficient of fuel rod bundle.

Equation (7) indicates that, addition of nanoparticles increases the thermal conductivity of the base fluid. This enhancement in thermal conductivity increases the convective heat transfer coefficient. Also, chaotic movement of the solid particles in the flow will disturb the thermal boundary layer formation on the wall surface of fuel rod bundle (walls of rods and shell). As a result of this disturbance, the development of the thermal boundary layer is delayed. Because higher heat transfer coefficients are obtained at the inlet region of the rod bundle, the delay in thermal boundary layer formation resulted by adding nanoparticles will enhance the mean heat transfer coefficient. At higher volume fractions of nanofluids, both the thermal conductivity of nanofluid and the disturbance effect of the solid nanoparticles will increase. Thus, nanofluids with higher volume fractions have higher convective heat transfer coefficients.

Pressure drop is an important factor in fuel rod bundle. The pressure drop and coolant pumping power are strongly related. Figure 18 shows total pressure drop in fuel rod bundle for nanoparticle diameter of 50nm at different volume fractions and different Reynolds numbers.

It is clear that a linear relationship exists between the pressure drop and volume fraction of nanoparticles. This figure obviously shows that enhancing nanoparticles volume fraction increases the pressure drop. According to Equation (10) the viscosity of nanofluids increases with increment of nanoparticles volume fraction. Enhancement of nanofluids viscosity increases the walls shear stress; therefore the pressure drop of fuel rod bundle will be increased.

Figure 19 shows the heat transfer coefficient of rod bundle for different nanoparticle diameters at $\phi = 1\%$.

It can be seen that the heat transfer coefficient increases with decreasing the diameter of nanoparticles. The contact surface between the solid particles and the fluid is enhanced with decreasing the diameter of particles, therefore the heat transfer coefficient increases.

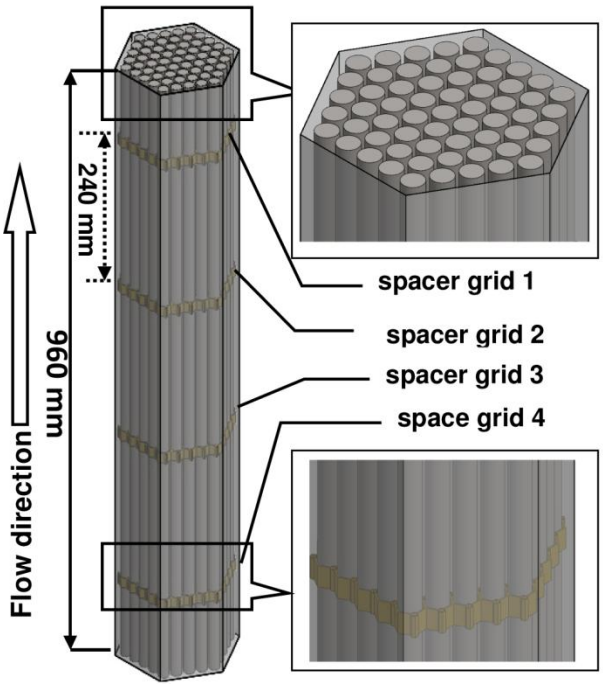

Figure 1: Full model of studied fuel rod bundle

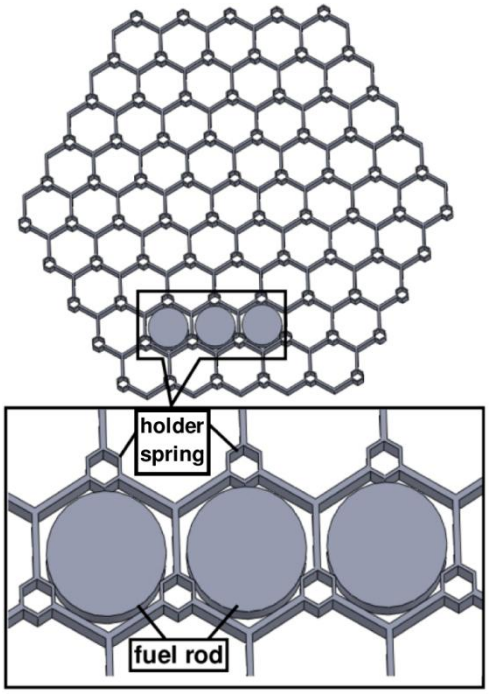

Figure 2: Full model of studied spacer grids

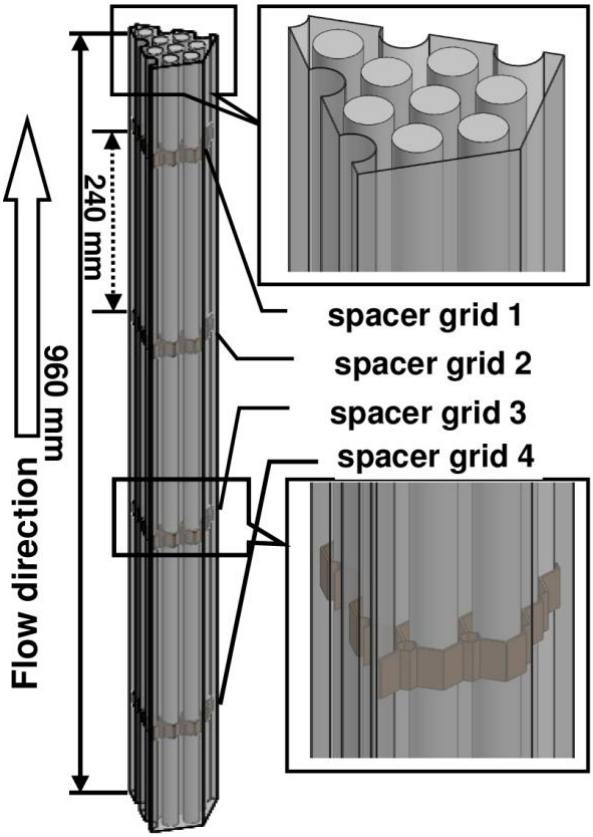

Figure 3: 60 degree segment of studied fuel rod bundle

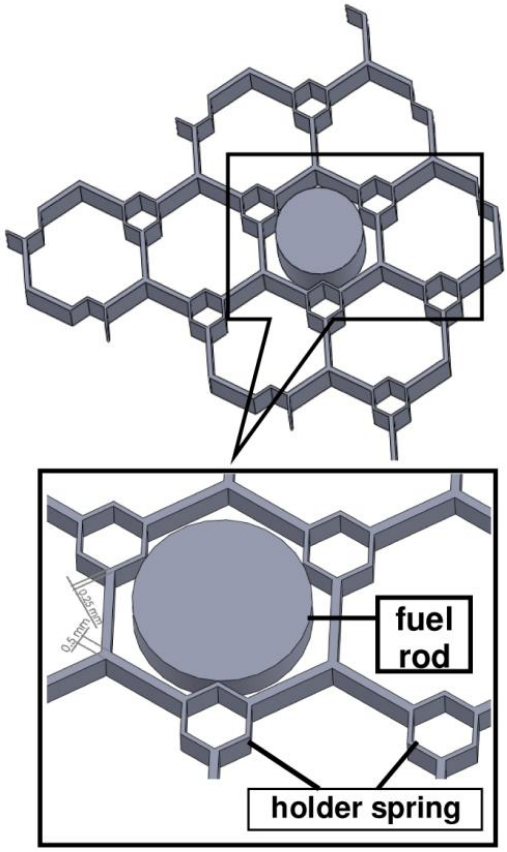

Figure 4: 60 degree segment of spacer grid

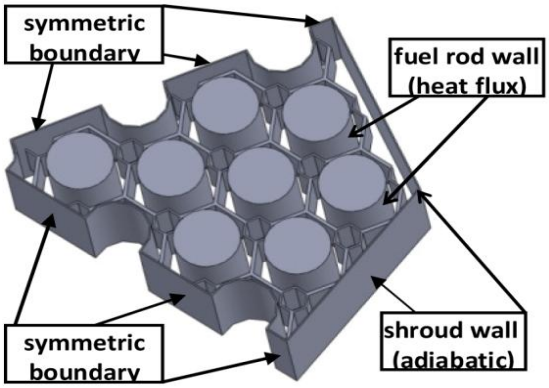

Figure 5: Some boundary conditions

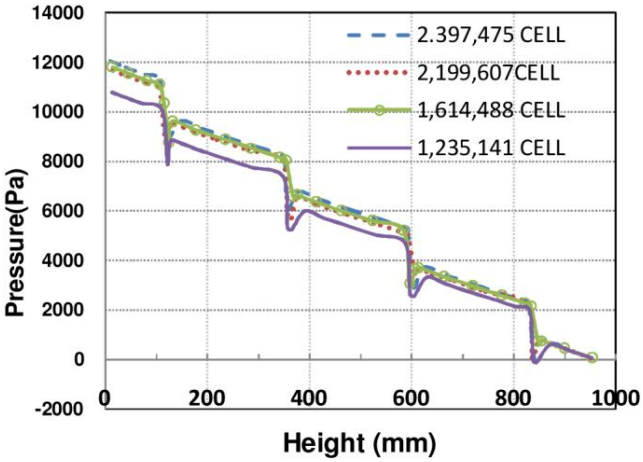

Figure 6: The cladding temperature of fuel rod bundle

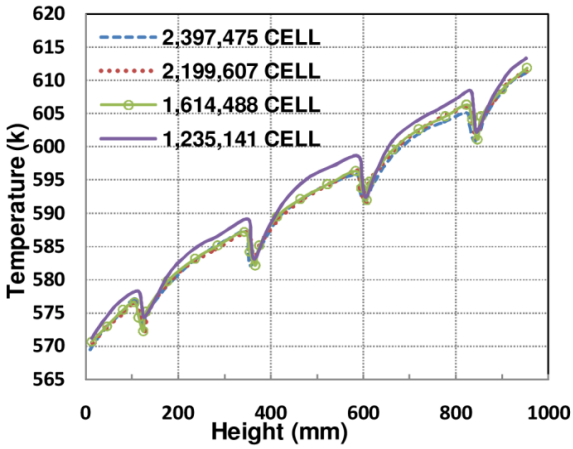

Figure 7: Pressure of coolant fluid in the flow direction

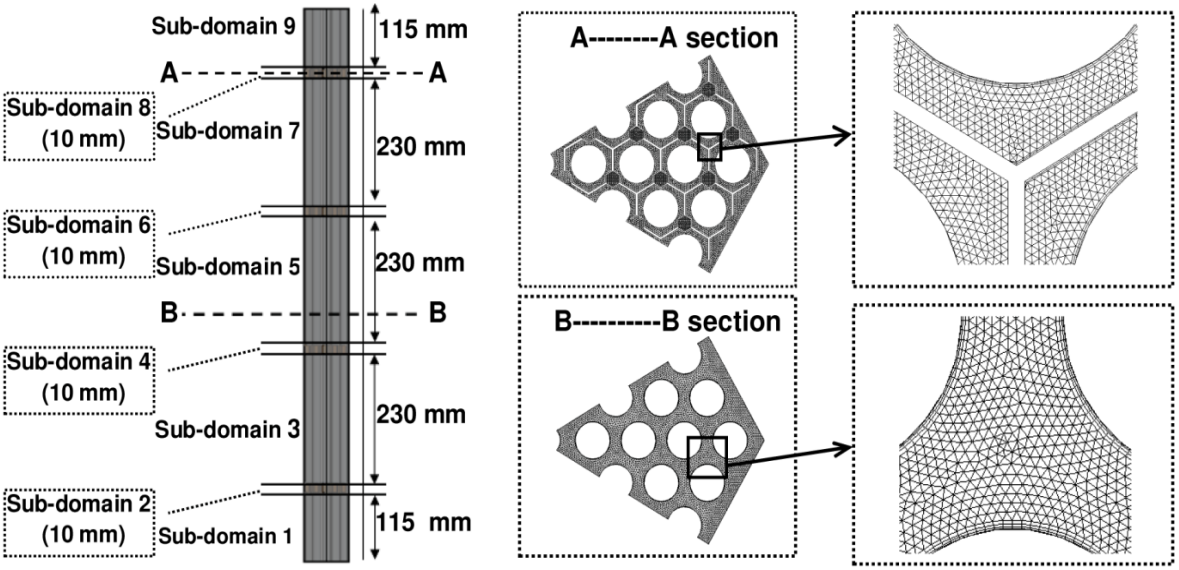

Figure 8: Mesh cross section in (A-----A) and (B-----B) regions .

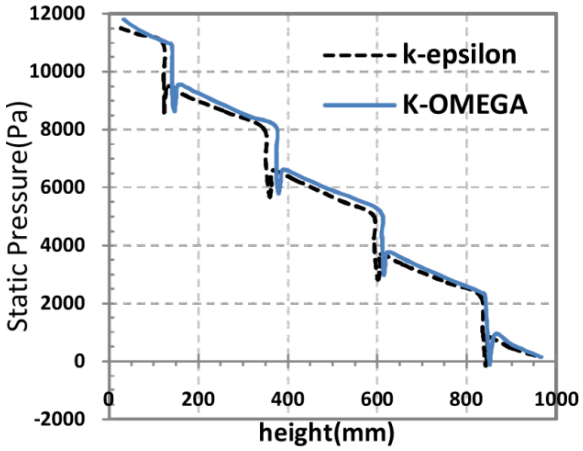

Figure 9: Average pressure of coolant fluid as a function of height

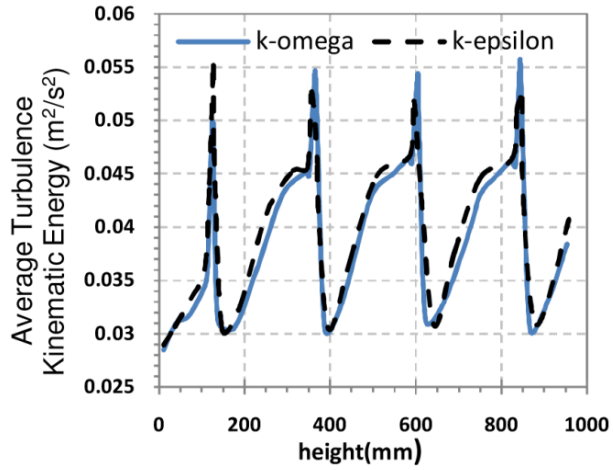

Figure 10: The average turbulent intensity as a function of height

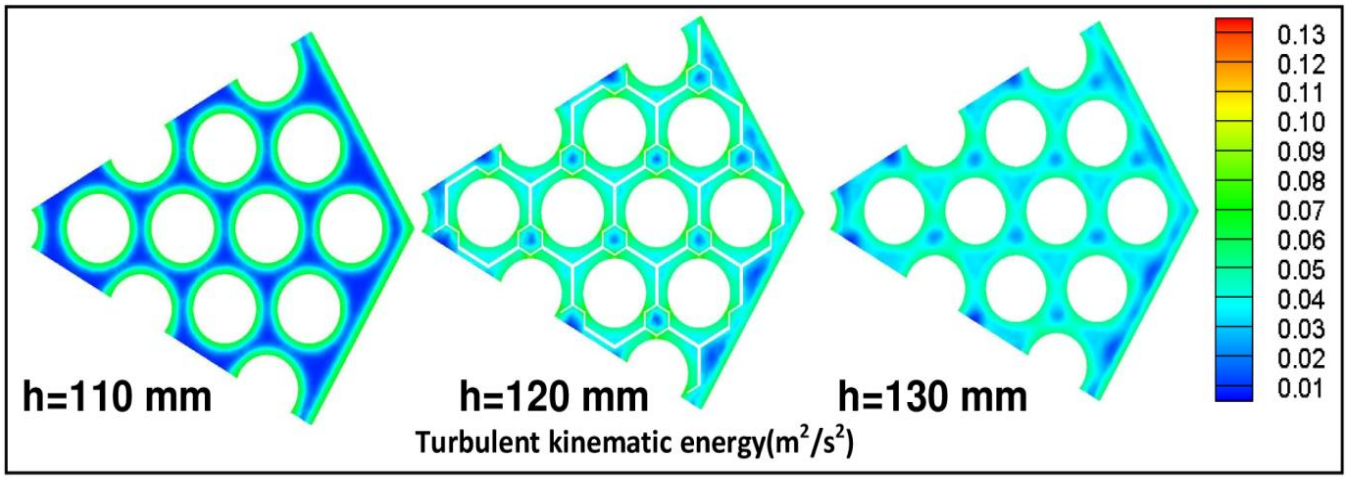

Figure 11: Contours of average turbulence kinetic energy in different heights($k-\omega$ SST model)

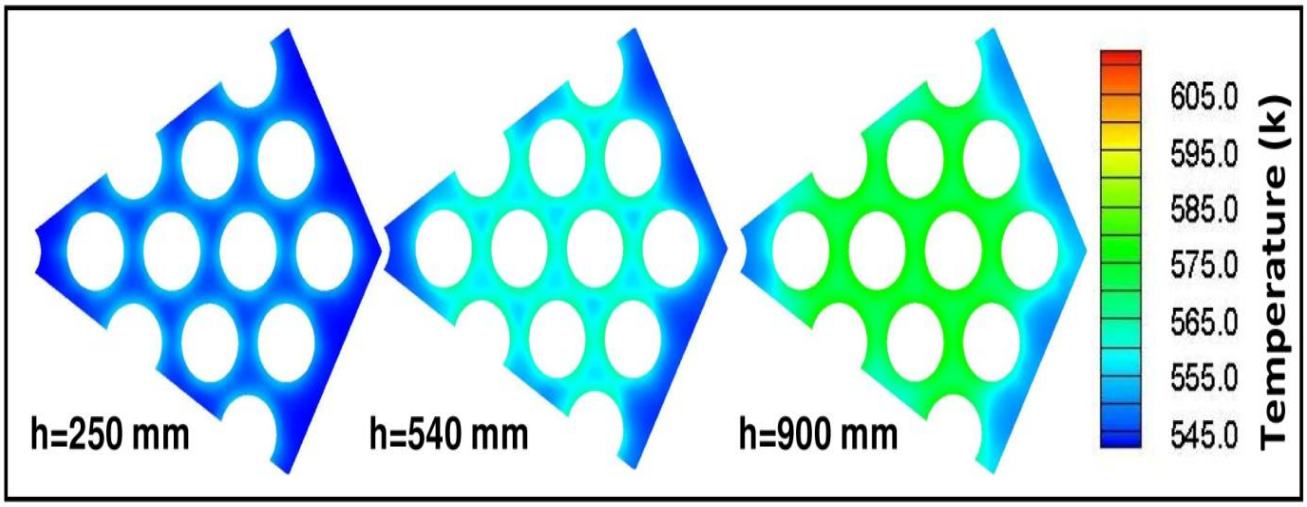

Figure 12: Contours of coolant fluid temperature in different heights($k-\omega$ SST model)

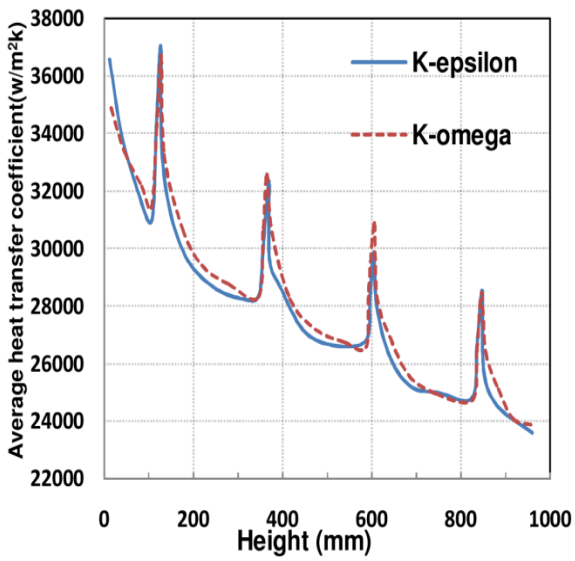

Figure 13: Heat transfer coefficient as a function of height

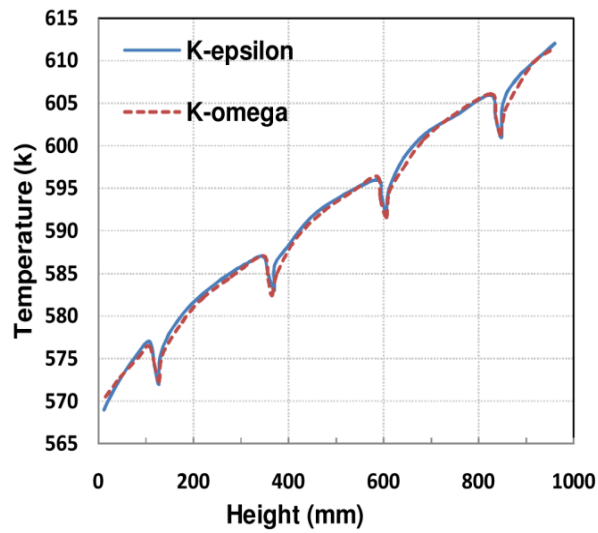

Figure 14: Average cladding temperature in flow direction

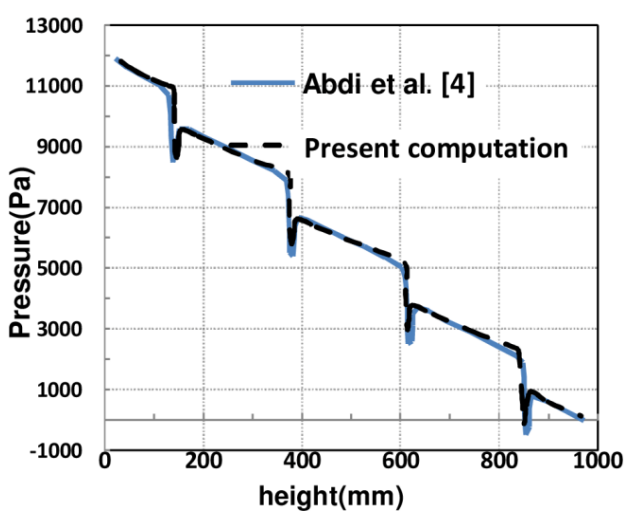

Figure 15: Pressure of coolant fluid in the flow direction

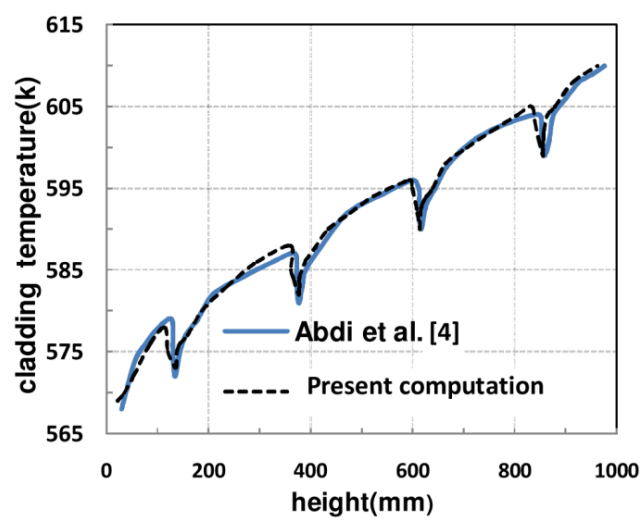

Figure 16: The cladding temperature of fuel rod bundle

Table 1: Thermo-physical properties of AL_2O_3 and water

	$\rho(kg/m^3)$	$C_P(kj/kg.K)$	$K(w/m^2.K)$
AL_2O_3	3970	1000	22
water	746	5268	0.5786

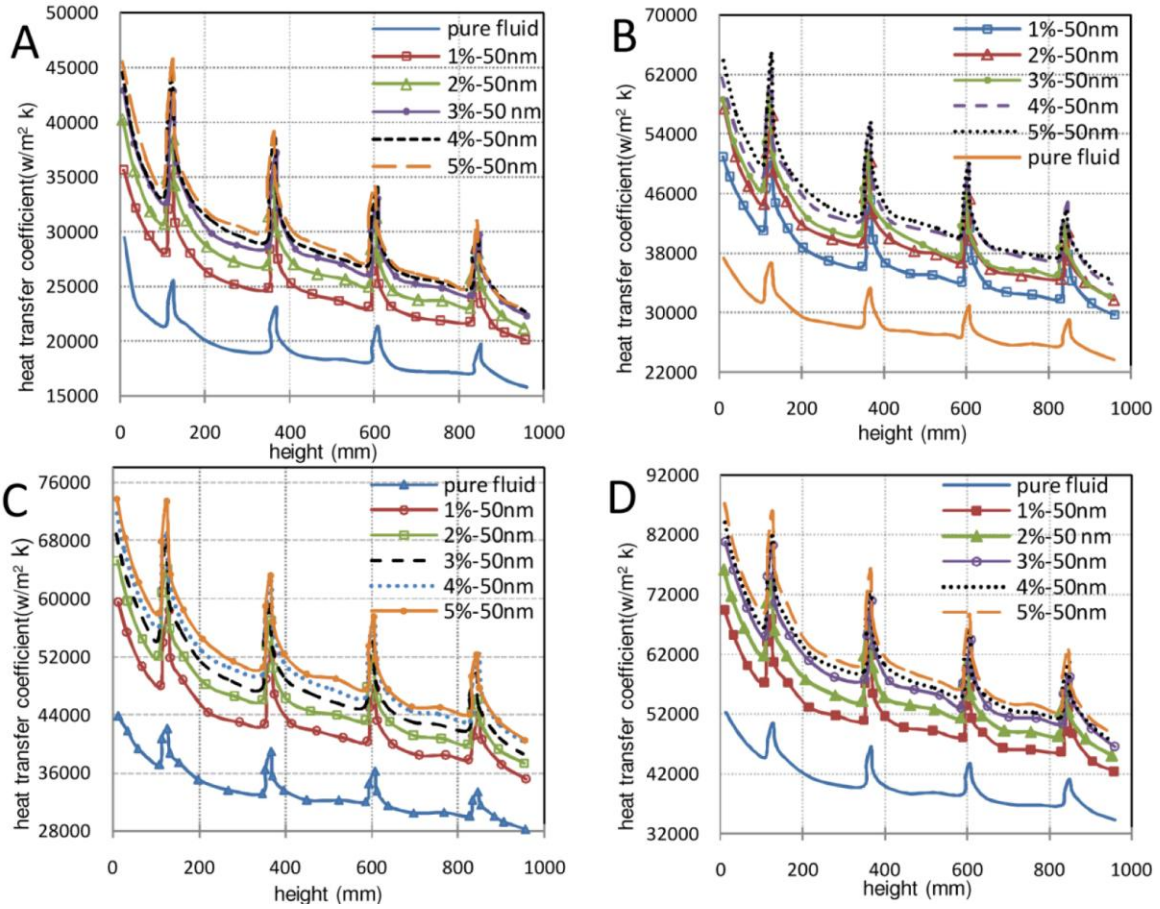

Figure 17: Heat transfer coefficient at d_p=50 nm at different Re ; a 125000; b 203000; c 250000;d 312000

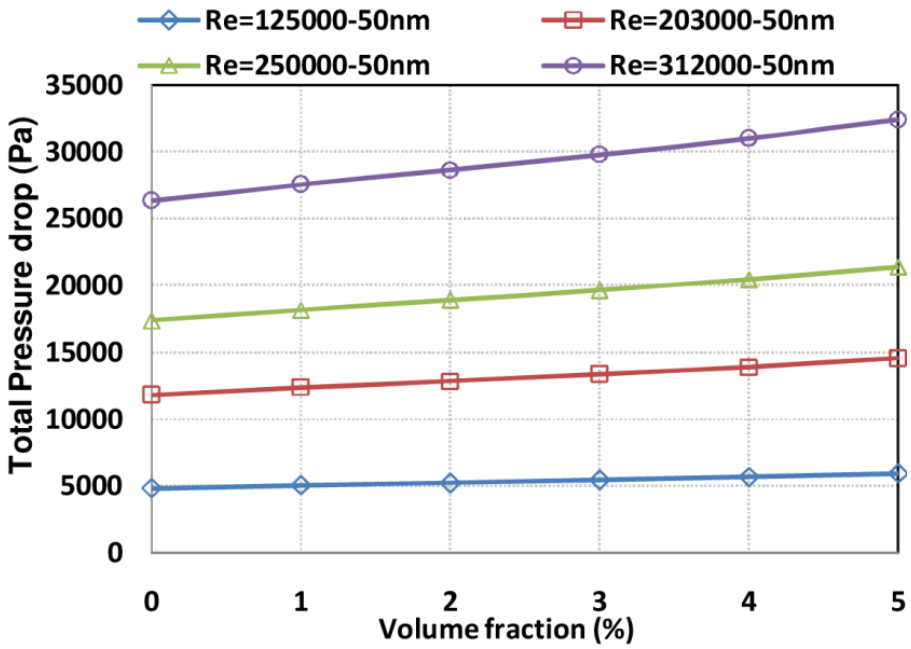

Figure 18: Total pressure drop in fuel rod bundle(d_p=50 nm)

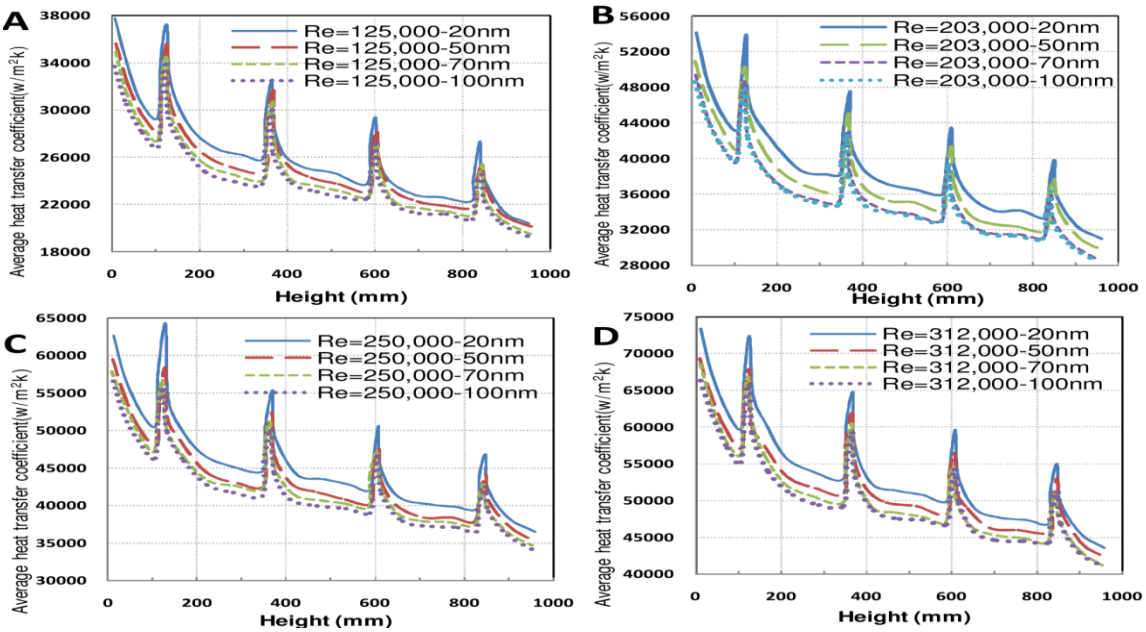

Figure 19: Heat transfer coefficient at $\phi = 1\%$ at different Re; a 125000; b 203000; c 250000;d 312000

Table 2: Mean heat transfer coefficient in rod bundle(d_p=50 nm)

Reynolds number	$\phi = 0\%$	$\phi = 1\%$	$\phi = 2\%$	$\phi = 3\%$	$\phi = 4\%$	$\phi = 5\%$
125000	20163	26566	29117	30595	31505	32304
203000	29264	38707	42347	43395	45508	46348
250000	34714	45288	48806	51248	53347	54532
312000	41886	53880	58091	60970	62738	64673

Table 3: Total pressure drop of fuel rod bundle (pa) at $\phi = 1\%$

Particle diameter	**Re= 125000**	**Re= 203000**	**Re= 250000**	**Re= 312000**
20 nm	5194	12717	18692	28316
50 nm	5024	12340	18162	27546
70 nm	5004	12297	18102	27457
100 nm	4992	12272	18064	27405

Table (3) shows the total pressure drop of rod bundle nanofluid at volume fraction of 0.01 at different particle diameters and different Reynolds numbers. Results show that by increasing the diameter of nanoparticles, the total pressure drop of rod bundle (difference between inlet pressure and outlet pressure) decreases. For example when the diameter of particles increases from 20 to 100 nm, total pressure drop decreases more than 3% at Re=235000. Chon *et al.*, (2005) correlation shows that by increasing the diameter of nanoparticles, the nanofluid viscosity decreases and viscosity reduction of nanofluids yields to lower pressure drop.

Conclusion

In this study the flow field and heat transfer characteristics of water-AL2O3 nanofluid in VVER-440 fuel rod bundle are numerically investigated. A 60 degree segment of fuel rod bundle consists of 12 fuel rods

(8 full rods and 4 half rods), central tube, 4 spacer grids and walls of shroud is considered for simulation. The results can be summarized as follow:

- Addition of Al_2O_3 nanoparticles in base fluid has a significant enhancement in heat transfer compared to that of the pure fluid. Although, the pressure drop for Nanofluids flow is slightly higher than the pressure drop for the pure water flow.
- Increasing nanoparticles volume fraction enhances the heat transfer coefficient. For example, at different Reynolds numbers, by increasing nanoparticles volume fraction from 0.0 to 0.01, the total average of the heat transfer coefficient increases between 28% to 32%.
- By enhancement of nanoparticles volume fraction, total pressure drop rises gradually. For example, at different Reynolds numbers, the increment of nanoparticles volume fraction from 0.0 to 0.05, yielded to the total pressure drop enhancement between 25% to 29%.
- At different Reynolds numbers, decreasing nanoparticles diameter leads to higher heat transfer coefficient.
- Decreasing nanoparticles diameter increases pressure drop. For example, at volume fraction of 1%, by decreasing nanoparticles diameter from 100 to 20 nm, the total pressure drop increases between 1% to 3% at different Reynolds numbers.

ACKNOWLEDGMENT
The authors gratefully acknowledge the financial support of the Iranian Nanotechnology Initiative Council.

REFERENCES

Abdi MR, Asgari M, Rezaee Ebrahim Saraee Kh and Talebi M (2012). Numerical Simulation of Split Vane in a 60 Fuel Rod Bundle of VVER-440 Reactor and Survey the Effect of Large Length Split Vane (LLSV) and Half-Length Split Vane (HLSV) on Heat Transfer Distribution, *World Applied Sciences Journal* **18**(7) 909-917.

Aszódi A and Tóth S (2008). CFD analysis of flow field in a triangular rod bundle, *Nuclear Engineering and Design* **21**(8) 352–363.

Behzadmehr A, Saffar-Avval M and Galanis N (2007). Prediction of turbulent forced convection of a nanofluid in a tube with uniform heat flux using a two phase approach, *International Journal of Heat and Fluid Flow* **28**(2) 211–219.

Buongiorno J and Truong B (2005). Preliminary study of water- based nanofluid coolants for PWRs, *Transactions of the American Nuclear Society* **92** 383–384.

Choi SUS (1995). Enhancing thermal conductivity of fluid with nanoparticles, developments and applications of non-Newtonian flow, *ASME FED **231**/MD* 6699–105.

Chon CH, Kihm KD, Lee SP and Choi SUS (2005). Empirical correlation finding the role of temperature and particle size for nanofluid (Al2O3) thermal conductivity enhancement, *Applied Physics Letters* **87** 153107–153110.

Conner ME, Baglietto E and Elmahdi AM (2010). CFD methodology and validation for single-phase flow in PWR fuel assemblies, *Nuclear Engineering and Design* **240** 2088–2095.

Cui XZ and Kim KY (2003). Three-Dimensional Analysis of Turbulent Heat Transfer and Flow through Mixing Vane in A Subchannel of Nuclear Reactor, *Journal of Nuclear Science and Technology* **40**(10) 719–724.

Eastman JA, Phillpot SR, Choi SUS and Keblinski P (2002). Eastman, Mechanisms of heat flow in suspensions of nano-sized particles (nanofluid), *International Journal of Heat Mass Transfer* **45** 855–863.

Eastman JA, Phillpot SR, Choi SUS and Keblinski P (2004). Thermal transport in nanofluids. *Annual Review of Materials Research* **34** 219–246.

Ghaffari O, Behzadmehr A and Ajam H (2010). Turbulent mixed convection of a nanofluid in a horizontal curved tube using a two-phase approach, *International Communications in Heat and Mass Transfer* **37**(10) 1551–1558.

Hadad K, Hajizadeh A, Jafarpour K and Ganapol BD (2010). Neutronic study of nanofluids application to VVER-1000, *Annals of Nuclear Energy* **37**(11) 1447–1455.
Janga SP and Choi SUS (2004). Role of Brownian motion in the enhanced thermal conductivity of nanofluids, *Applied Physics Letters* **84** 4316-4318.
Ltd O (2011). User guide, Available: http://www.openfoam.com /docts/user.
Masoumi N, Sohrabi N and Behzadmehr A (2009). New Model for Calculating the Effective Viscosity of Nanofluids. *Journal of Physics D: Applied Physics* 42 55501–55506.
Mintsa HA, Roy G, Nguyen CT and Doucet D (2009). New Temperature Dependent Thermal Conductivity Data for Water-Based Nanofluids, *International Journal of Thermal Science* **48** 363–371.
Pak BC and Cho YI (1998). Hydrodynamic and Heat Transfer Study of Dispersed Fluids with Submicron Metallic Oxide Particles, *Experimental Heat Transfer* 11151–170.
Soo SB (2009). CHF experiment and CFD analysis in a 2×3 rod bundle with mixing vane, *Nuclear Engineering and Design* **239** 899–912.
TóthAszódi SA (2006). Calculations of coolant flow in a VVER-440 fuel bundle with the code ANSYS CFX 10.0, Proceedings of the Workshop on Modeling and Measurements of Two-Phase Flows and Heat Transfer in Nuclear Fuel Assemblies, *Stockholm, Sweden*.
Zarifi E, Jahanfarnia G and Veysi F (2013). Thermal–hydraulic modeling of nanofluids as the coolant in VVER-1000 reactor core by the porous media approach, *Annals of Nuclear Energy* **51** 203–212.